Longitudinal Legendre polynomial expansion of electromagnetic fields for analysis of arbitrary-shaped gratings

Amin Khavasi, Ali Kazemi Jahromi, and Khashayar Mehrany*

Department of Electrical Engineering, Sharif University of Technology, P.O. Box 11365-9363, Tehran, Iran
**Corresponding author: mehrany@sharif.edu*

Received February 4, 2008; revised April 9, 2008; accepted April 13, 2008;
posted April 21, 2008 (Doc. ID 92453); published June 9, 2008

The Legendre polynomial expansion method (LPEM), which has been successfully applied to homogenous and longitudinally inhomogeneous gratings [J. Opt. Soc. Am. B **24**, 2676 (2007)], is now generalized for the efficient analysis of arbitrary-shaped surface relief gratings. The modulated region is cut into a few sufficiently thin arbitrary-shaped subgratings of equal spatial period, where electromagnetic field dependence is now smooth enough to be approximated by keeping fewer Legendre basis functions. The *R*-matrix propagation algorithm is then employed to match the Legendre polynomial expansions of the transverse electric and magnetic fields across the upper and lower interfaces of every slice. The proposed strategy then enhances the overall computational efficiency, reduces the required memory size, and permits the efficient study of arbitrary-shaped gratings. Here the rigorous approach is followed, and analytical formulas of the involved matrices are given.

OCIS codes: 050.2770, 050.1950, 050.7330, 000.3860.

1. INTRODUCTION

Arbitrarily shaped surface relief gratings are among the most difficult to analyze, owing to the longitudinal inhomogeneity along their grooves, and yet find promising potentiality in a wide range of applications, e.g., in integrated optics, nanophotonics, quantum electronics, and spectroscopy [1]. It is therefore essential to have a fast, simple, rigorous, stable, and versatile method to deal with these structures. The rigorous coupled-wave analysis (RCWA) is one of the simplest and most well-liked methods, which was popularized by Moharam and Gaylord about 30 years ago [2,3]. This method yields a set of coupled differential equations, which can be easily transformed into a simple eigenvalue problem for lamellar gratings. It is also applicable for the analysis of successive lamellar structures, which can represent the staircase approximation of an arbitrary-shaped surface relief grating. Although originally facing numerical instabilities in the analysis of deep gratings, the method was soon redeemed by employing the *R*-matrix propagation algorithm, scattering matrix method [4], and enhanced transmittance matrix approach [5]. The remaining problem was then to find a fast converging formulation in the analysis of metallic gratings in TM polarization. This was also done using the correct Fourier factorization technique, which brought forth spectacular results [6–8]. The RCWA is therefore among the most suitable techniques available for the analysis of lamellar dielectric and/or metallic gratings. In the analysis of arbitrarily shaped gratings, however, this method inevitably relies on the staircase approximation, whose accuracy has been impugned in a fairly recent paper, where it has been shown that using the staircase approximation renders some nonalgorithmic artifacts in TM polarization [9].

This problem can be overcome by applying the differential method (DM), which employs numerical integration to solve almost the same set of coupled differential equations governing the transverse electromagnetic field dependence in the vertical direction along the grooves. Once the convergence rate of the DM is improved by employing the fast Fourier factorization (FFF) technique [10,11], it can effectively analyze almost all common grating structures. Still, two remaining problems are to be faced. First, the numerical integration of a large set of equations could be time consuming and computationally burdensome. Second, numerical instabilities are likely to be encountered in the analysis of thick gratings, for which either the *S*-matrix or *R*-matrix propagation algorithm is needed to break up the whole structure into sufficiently thin slices [10].

One other approach to successfully analyze surface relief gratings is the coordinate transformation method developed by Chandezon *et al.* (C-method) [12]. Although this method outsmarts the RCWA in the analysis of surface relief gratings [13], it has two intrinsic problems that make it inappropriate for some important structures. First, the convergence of the formulation is somewhat slow for surface relief gratings with sharp edges [14]. This problem, which can be subdued by applying the adaptive spatial resolution technique (ASR) [15], is especially pronounced whenever the slope of the surface relief profile tends to infinity, e.g., in binary gratings. Second, it is not

directly applicable to volume gratings and surface relief gratings whose grooves are filled with inhomogeneous materials [16,17].

More recently, a nonmodal method by Fourier expansion has been introduced, where the RCWA formulation is combined with Galerkin's method, and Maxwell's equations in Fourier space are analytically projected onto the Hilbert space spanned by the Legendre polynomial basis functions [17,18]. In this fashion, the RCWA set of coupled differential equations is converted to a well-behaved algebraic system of equations, thanks to which it is possible to dispense with the conventional propagation algorithms that would be otherwise necessary for circumventing numerical difficulties associated with the presence of growing evanescent waves. This approach, here being referred to as the Legendre polynomial expansion method (LPEM), is particularly effective in the analysis of a special category of longitudinally inhomogeneous gratings for which the permittivity profile $\epsilon(x,z)$ happens to be separable in the Cartesian coordinate system, i.e., $\epsilon(x,z)=\epsilon_x(x)\epsilon_z(z)$ [18]. This is not, however, the most general case that can arise in the analysis of arbitrary-shaped gratings. In particular, a large number of Legendre polynomial terms is needed to accurately approximate the harmonically rich Floquet orders of deep surface relief gratings. This problem, which evokes burdensome memory and time-consuming computations, especially for metallic gratings in TM polarization, is here tackled by cutting the structure into successive sufficiently thin slices. In each slice, then, the electromagnetic field dependence of space harmonics is smooth enough to be approximated by keeping only a few Legendre polynomial terms. In this fashion, the size of the involved matrices dwindles away and no heavy computational burden is incurred. To this end, a duly adapted R-matrix propagation algorithm is here proposed, and a new effective approach based on the LPEM is devised for the analysis of arbitrary-shaped gratings. The decomposition of the modulated area into a few slices is shown to be indispensable for metallic gratings illuminated by TM-polarized plane waves, for which the LPEM becomes too time consuming to be of practical use unless the whole structure is represented by a stack of a few arbitrary-shaped subgratings of equal spatial period. In this latter case, the FFF rule is also applied to ensure the fast convergence of the proposed formulation.

This paper is organized as follows: The formulation of the proposed method for both major polarizations is presented in Section 2, where the proper R-matrix propagation algorithm for this nonmodal technique is introduced for what we believe to be the first time. Several numerical examples are then given in the following sections, where the proposed technique is compared with the most popular methods available for the analysis of arbitrary-shaped gratings, i.e., the DM, the RCWA, and the C-method. Plots of convergence of diffraction efficiencies are presented versus the number of dividing slices and the number of retained Legendre polynomial terms. The energy balance criterion and the validity of the reciprocity theorem are also numerically tested, and a metallic grating with resonant anomalies is analyzed. In comparison with the DM and the RCWA algorithm, the presented approach is numerically shown to be superior in performance. In comparison with the C-method, on the other hand, the proposed technique is shown to be superior in generality and versatility. Conclusions are finally made in Section 5.

2. FORMULATION

A typical arbitrary-shaped surface relief grating is depicted in Fig. 1, where the grating profile is described by an arbitrary yet periodic function $f(x)$,

$$f(x+\Lambda_G)=f(x), \tag{1}$$

where Λ_G is the grating period.

It is quite well known that the normalized electric field vector outside the grating region can be expressed by the following Rayleigh expansion:

$$\boldsymbol{E}_1=\hat{u}e^{-j\mathbf{k}_{10}\cdot\mathbf{r}}+\sum_{i=-\infty}^{+\infty}\boldsymbol{R}_i e^{-j\mathbf{k}_{1i}\cdot\mathbf{r}} \tag{2}$$

for $z<0$ in region 1, and

$$\boldsymbol{E}_3=\sum_{i=-\infty}^{+\infty}\boldsymbol{T}_i e^{-j\mathbf{k}_{3i}\cdot(\mathbf{r}-d\hat{z})} \tag{3}$$

for $z>d$ in region 3.

In these expressions, $\mathbf{r}=x\hat{x}+z\hat{z}$, $\boldsymbol{k}_{1i}=k_{xi}\hat{x}+k_{z1i}\hat{z}$, and $\boldsymbol{k}_{3i}=k_{xi}\hat{x}+k_{z3i}\hat{z}$, where

$$k_{xi}=k_1\sin\alpha-i\frac{2\pi}{\Lambda_G}, \tag{4}$$

$$k_{zli}=\sqrt{k_l^2-k_{xi}^2},\quad k_l=\frac{2\pi}{\lambda}n_l \tag{5}$$

for $l=1,3$ (representing regions 1 or 3).

The index i, which is running from $-\infty$ to $+\infty$, stands for the ith space harmonic corresponding to the ith backward-diffracted order in region 1, $(z<0)$ and the forward-diffracted order in region 3, $(z>d)$. The $\boldsymbol{R}_i$ and $\boldsymbol{T}_i$ coefficients denote the normalized electric field vector of the ith reflected and transmitted Floquet order, respectively. The z component of the wave vector, k_{z1i} is either negative real (propagating wave) or positive imaginary

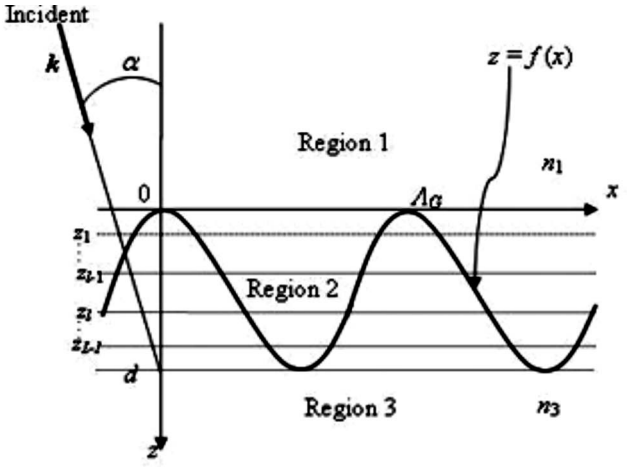

Fig. 1. Geometry of a typical surface relief grating represented as a stack of L arbitrary-shaped subgratings.

(evanescent wave). Likewise, for region 3, k_{z3i}, is either positive real (a propagating wave) or negative imaginary (an evanescent wave). Furthermore, $\hat{u}$ stands for the incident-wave polarization unit vector and is given by

$$\hat{u} = \begin{cases} \hat{y} & \text{TE} \\ \cos\alpha\hat{x} - \sin\alpha\hat{z} & \text{TM} \end{cases}. \tag{6}$$

Inside the grating area ($0<z<d$), on the other hand, the electric and magnetic fields are both pseudoperiodic and can be expressed in terms of coupled space harmonics governed by a set of ordinary differential equations [19]. This set of equations is here solved by using Galerkin's method with Legendre polynomial basis functions. To this end, the overall structure is divided into L successive slices of planar gratings where, within each slice, the electromagnetic field dependence is found in terms of fewer Legendre basis functions. The above-mentioned division of the structure into multilevel arbitrary-shaped subgratings, however, should not be confused with the conventional staircase approximation, where the individual layers are sufficiently thin to be considered uniform binary index gratings.

In the following subsections, therefore, we will find a set of algebraic equations governing the electromagnetic field dependence of both major polarizations inside the grating region, within the lth arbitrary-shaped subgrating between z_{l-1} and z_l. We will then propose an adapted R-matrix algorithm to fully solve the problem.

A. TE Polarization

In accordance with the Floquet theorem, TE-polarized electromagnetic fields within the grating can be written in terms of the coupled space harmonics:

$$\mathbf{E} = \sum_i [S_{yi}(z)\hat{y}]\exp(-jk_{xi}x), \tag{7}$$

$$\mathbf{H} = \sqrt{\frac{\epsilon_0}{\mu_0}}\sum_i [U_{xi}(z)\hat{x} + U_{zi}(z)\hat{z}]\exp(-jk_{xi}x). \tag{8}$$

Substitution of Eqs. (7) and (8) into Maxwell's equations then renders the following set of ordinary differential equations:

$$\frac{dS_{yi}(z)}{dz} = jk_0U_{xi}(z), \tag{9}$$

$$\frac{dU_{xi}(z)}{dz} = jk_0\left[-\left(\frac{k_{xi}}{k_0}\right)^2 S_{yi}(z) + \sum_p \epsilon_{i-p}(z)S_{yp}(z)\right], \tag{10}$$

or in the concise matrix form,

$$\frac{d[S_y(z)]}{dz} = jk_0\mathbf{I}[U_x(z)], \tag{11}$$

$$\frac{d[U_x(z)]}{dz} = jk_0\left([[\epsilon]] - \left(\frac{\mathbf{K_x}}{k_0}\right)^2\right)[S_y(z)], \tag{12}$$

where $\mathbf{I}$ is the identity matrix, $\mathbf{K_x}$ is a diagonal matrix whose (i,i) element is k_{xi}, $\epsilon_m(z)$ denotes the mth Fourier coefficient of $\epsilon(x,z)$, $[[\epsilon]]$ represents a Toeplitz matrix with the (i,p) entry being equal to $\epsilon_{i-p}(z)$, $[S_y(z)]$ is a column vector constructed by $S_{yi}(z)$ functions, and $[U_x(z)]$ is a column vector constructed by $U_{xi}(z)$ functions.

This set of linear differential equations can now be transformed into an algebraic system of equations by following Galerkin's method, i.e., by expanding the coupled space harmonics in terms of Legendre polynomial basis functions:

$$S_{yi}(z) = \sum_{m=0}^{+\infty} h_m^i P_m(\xi), \tag{13}$$

$$U_{xi}(z) = \sum_{m=0}^{+\infty} t_m^i P_m(\xi). \tag{14}$$

Here $\xi=[2(z-z_{l-1})-d_l]/d_l$ is a scaling factor, $P_m(\xi)$ stands for the mth normalized Legendre polynomial, and d_l denotes the thickness of the lth layer shown in Fig. 1.

The above-mentioned polynomial expansion of space harmonics as given in Eqs. (13) and (14) is substituted in Eqs. (9) and (10):

$$\left(\frac{2}{d_l}\right)\sum_m h_m^i P'_m(\xi) - jk_0\sum_m t_m^i P_m(\xi) = 0, \tag{15}$$

$$\left(\frac{2}{d_l}\right)\sum_m t_m^i P'_m(\xi) + jk_0\sum_m P_m(\xi)\left[\left(\frac{k_{xi}}{k_0}\right)^2 h_m^i - \sum_p \epsilon_{i-p}(\xi)h_m^p\right] = 0, \tag{16}$$

where $P'_m(\xi)$ is the derivative of $P_m(\xi)$.

The resultant equation should then be analytically projected onto the Hilbert space spanned by the Legendre polynomials:

$$\left(\frac{2}{d_l}\right)\sum_m h_m^i\langle P_n,P'_m\rangle - jk_0\sum_m t_m^i\langle P_n,P_m\rangle = 0, \tag{17}$$

$$\left(\frac{2}{d_l}\right)\sum_m t_m^i\langle P_n,P'_m\rangle + j\frac{k_{xi}^2}{k_0}\sum_m \left(h_m^i\langle P_n,P_m\rangle - jk_0 \times \sum_p h_m^p\langle P_n,\epsilon_{i-p}P_m\rangle\right) = 0, \tag{18}$$

where $\langle f,g\rangle=\int_{-1}^{1} f(\xi)g(\xi)d\xi$ stands for the inner product of any two arbitrary functions in $L_2(-1,1)$ and consequently

$$\langle P_n,P_m\rangle = \begin{cases} 0 & m \neq n \\ \dfrac{2}{2m+1} & m = n \end{cases}, \tag{19}$$

$$\langle P_n,P'_m\rangle = \begin{cases} 2 & m-n = \text{odd},\ m-n>0, \\ 0 & \text{oth} \end{cases} \tag{20}$$

and $\langle P_n,\epsilon_{i-p}(\xi)P_m\rangle$ should be numerically calculated.

All the summations in these expressions should be inevitably truncated; therefore, the indices of summations m, n, and i are here assumed to run from 0 to $M-1$, 0 to $M-2$, and $-N$ to N, respectively. This gives rise to a set of

$2(2N+1)(M-1)$ independent equations with $2M(2N+1)$ unknown coefficients, which can be be arranged in the concise matrix form

$$\mathbf{Q}^{TE}\begin{bmatrix}[\bar{h}_m^i]\\ [\bar{t}_m^i]\end{bmatrix}=\mathbf{0}, \tag{21}$$

where $\mathbf{Q}^{TE}$ is a $2(2N+1)(M-1)\times 2(2N+1)M$ matrix given in Appendix A and $[\bar{q}_m^i]$ and $[\bar{t}_m^i]$ are column vectors whose $(i+N)M+m+1$ element is h_m^i and t_m^i, respectively.

The missing equations can be found once the appropriate boundary conditions, i.e., the continuity of the transverse electric and magnetic fields across the upper and lower interfaces of the lth slice at $z=z_{l-1}$ and $z=z_l$, are duly applied. This is done in Subsection 2.C, where each layer is represented by a layer $\tilde{\mathbf{r}}^{(l)}$ matrix [4].

B. TM Polarization

Similarly, TM-polarized electromagnetic fields in the modulated region can be written as follows:

$$\boldsymbol{E}=\sum_i [S_{xi}(z)\hat{x}+S_{zi}(z)\hat{z}]\exp(-jk_{xi}x), \tag{22}$$

$$\boldsymbol{H}=\sqrt{\frac{\epsilon_0}{\mu_0}}\sum_i [U_{yi}(z)\hat{y}]\exp(-jk_{xi}x). \tag{23}$$

In TM polarization, however, the inevitable truncation of the Fourier-based expansions and the discontinuity of the permittivity profile can considerably slow down the convergence rate of the Floquet expansion. Consequently, the FFF rule should be applied to appropriately resolve the issue [11]. This results in the following set of coupled ordinary differential equations:

$$\frac{\mathrm{d}}{\mathrm{d}z}\begin{bmatrix}[S_x]\\ [U_y]\end{bmatrix}=-\begin{bmatrix}\mathbf{M}^{TM11} & \mathbf{M}^{TM12}\\ \mathbf{M}^{TM21} & \mathbf{M}^{TM22}\end{bmatrix}\begin{bmatrix}[S_x]\\ [U_y]\end{bmatrix}, \tag{24}$$

$$\mathbf{M}^{TM11}=\mathbf{K_x}\mathbf{G}\mathbf{B}, \tag{25}$$

$$\mathbf{M}^{TM12}=\mathbf{K_x}\mathbf{G}\mathbf{K_x}/k_0+jk_0\mathbf{I}, \tag{26}$$

$$\mathbf{M}^{TM21}=jk_0(\mathbf{A}+[[1/\epsilon]]^{-1}-j\mathbf{B}\mathbf{G}\mathbf{B}), \tag{27}$$

$$\mathbf{M}^{TM22}=\mathbf{B}\mathbf{G}\mathbf{K_x}, \tag{28}$$

where $[[1/\epsilon]]$ represents a Toeplitz matrix whose (i,p) element is $\epsilon_{i-p}^{-1}(z)$, $[S_x]$ is a column vector constructed by $S_{xi}(z)$ functions, $[U_y]$ is a column vector constructed by $U_{yi}(z)$ functions, and

$$\mathbf{\Delta}=[[\epsilon]]-[[1/\epsilon]]^{-1}, \tag{29}$$

$$\mathbf{A}=\mathbf{\Delta}[[c^2]], \tag{30}$$

$$\mathbf{B}=\mathbf{\Delta}[[cs]], \tag{31}$$

$$\mathbf{G}=-j([[\epsilon]]-\mathbf{A})^{-1}. \tag{32}$$

In these expressions, $[[c]]$ and $[[s]]$ stand for the Toeplitz matrices whose (i,p) elements are the $(i-p)$th Fourier coefficient of the $c(x)$ and $s(x)$ functions, respectively, where $c(x)=\cos\theta(x)$, $s(x)=\sin\theta(x)$, and $\theta(x)=\tan^{-1}\mathrm{d}f/\mathrm{d}x$.

Once again, the preceding set of ordinary differential equations should be projected onto the linear space spanned by the Legendre basis functions. Each space harmonic is therefore expanded in terms of the Legendre polynomials,

$$S_{xi}(z)=\sum_{m=0}^{+\infty} q_m^i P_m(\xi), \tag{33}$$

$$U_{yi}(z)=\sum_{m=0}^{+\infty} l_m^i P_m(\xi), \tag{34}$$

and the following set of algebraic equations is obtained:

$$\sum_m\left(q_m^i\frac{2}{d_l}\langle P_n,P_m'\rangle+\sum_p q_m^p\langle P_n,\mathbf{M}_{ip}^{TM11}P_m\rangle+\sum_p l_m^p\langle P_n,\mathbf{M}_{ip}^{TM12}P_m\rangle\right)=0, \tag{35}$$

$$\sum_m\left(l_m^i\frac{2}{d_l}\langle P_n,P_m'\rangle+\sum_p l_m^p\langle P_n,\mathbf{M}_{ip}^{TM22}P_m\rangle+\sum_p q_m^p\langle P_n,\mathbf{M}_{ip}^{TM21}P_m\rangle\right)=0. \tag{36}$$

Here, in contrast to the TE polarization, all the inner product terms should be numerically integrated. The only exception is the $\langle P_n,P_m'\rangle$ term, which is analytically given in Eq. (20).

In the same way, all the summations in these expressions should be inevitably truncated; i.e., the indices of summations m, n, and i run from 0 to $M-1$, 0 to $M-2$, and $-N$ to N, respectively. Therefore, the above-mentioned algebraic equations can be recast in the following matrix form:

$$\mathbf{Q}^{TM}\begin{bmatrix}[\bar{q}_m^i]\\ [\bar{l}_m^i]\end{bmatrix}=\mathbf{0}, \tag{37}$$

where $\mathbf{Q}^{TM}$ is a $2(2N+1)(M-1)\times 2(2N+1)M$ matrix given in Appendix A and $[\bar{q}_m^i]$ and $[\bar{l}_m^i]$ are column vectors whose $(i+N)M+m+1$ element is q_m^i and l_m^i, respectively.

This leaves us with $2(2N+1)$ missing equations, which are to be found by applying the appropriate boundary conditions. This is done in the next subsection, where each layer is represented by its corresponding R matrix.

C. *R*-Matrix Algorithm

In this subsection, the R-matrix propagation algorithm is given for TM polarization, where the transverse electric S_x and magnetic fields U_y are linked across every two adjacent layers and a layer r matrix, $\tilde{\mathbf{r}}^{(l)}$, is affixed to the lth interface:

$$\begin{bmatrix} [S_x(z_l)] \\ [S_x(z_{l-1})] \end{bmatrix} = \tilde{\mathbf{r}}^{(l)TM} \begin{bmatrix} [U_y(z_l)] \\ [U_y(z_{l-1})] \end{bmatrix}. \tag{38}$$

Analysis of the TE polarization follows the same line, where S_x and U_y are changed to S_y and U_x, respectively.

On the other hand, each space harmonic at $z=z_{l-1}$ and $z=z_l$ is already expanded in terms of the Legendre polynomial coefficients

$$\boldsymbol{\chi} \begin{bmatrix} [\bar{q}_m^i] \\ [\bar{l}_m^i] \end{bmatrix} = \begin{bmatrix} [U_y(z_l)] \\ [U_y(z_{l-1})] \end{bmatrix}, \tag{39}$$

$$\boldsymbol{\psi} \begin{bmatrix} [\bar{q}_m^i] \\ [\bar{l}_m^i] \end{bmatrix} = \begin{bmatrix} [S_x(z_l)] \\ [S_x(z_{l-1})] \end{bmatrix}, \tag{40}$$

where $\boldsymbol{\chi}$ and $\boldsymbol{\psi}$ matrices are obtained by using Eqs. (33) and (34). Further details are given in Appendix A.

Now, combining these two latter sets of equations together with that of Eq. (37) can render the required $\tilde{\mathbf{r}}^{(l)}$ matrix:

$$\tilde{\mathbf{r}}^{(l)TM} = \boldsymbol{\psi} \begin{bmatrix} \mathbf{Q}^{TM}_{(2(2N+1)(M-1))\times(2(2N+1)M)} \\ \hline \boldsymbol{\chi}_{(2(2N+1))\times(2(2N+1)M)} \end{bmatrix}^{-1} \times \begin{bmatrix} \mathbf{0}_{(2(2N+1)(M-1))\times(2(2N+1))} \\ \hline \mathbf{I}_{(2(2N+1))\times(2(2N+1))} \end{bmatrix}. \tag{41}$$

Once the layer r matrix is obtained, the following set of recursion formulas can be used to obtain the stack R matrix [4]:

$$\mathbf{R}_{11}^{(l)} = \tilde{\mathbf{r}}_{11}^{(l)} - \tilde{\mathbf{r}}_{12}^{(l)} \mathbf{Z}^{(l)} \tilde{\mathbf{r}}_{21}^{(l)},$$

$$\mathbf{R}_{12}^{(l)} = \tilde{\mathbf{r}}_{12}^{(l)} \mathbf{Z}^{(l)} \mathbf{R}_{12}^{(l-1)},$$

$$\mathbf{R}_{21}^{(l)} = -\mathbf{R}_{21}^{(l-1)} \mathbf{Z}^{(l)} \tilde{\mathbf{r}}_{21}^{(l)},$$

$$\mathbf{R}_{22}^{(l)} = \mathbf{R}_{22}^{(l-1)} + \mathbf{R}_{21}^{(l-1)} \mathbf{Z}^{(l)} \mathbf{R}_{12}^{(l-1)}, \tag{42}$$

where

$$\mathbf{Z}^{(l)} = (\tilde{\mathbf{r}}_{22}^{(l)} - \mathbf{R}_{11}^{(l-1)})^{-1}, \tag{43}$$

and the recursion process is initialized by setting $\mathbf{R}^{(1)} = \tilde{\mathbf{r}}^{(1)}$.

The overall R matrix should then be matched to the Rayleigh expansion without the modulated area, where the unknown $\boldsymbol{R}_i$ and $\boldsymbol{T}_i$ coefficients, i.e., diffracted field amplitudes, can be easily determined. In this fashion, the overall diffraction efficiencies can be easily calculated [18].

It should be noticed, however, that numerical overflow is not expected in the LPEM, where forward and backward exponential evanescent orders are absent and consequently the presented R-matrix propagation algorithm is not necessary to secure the numerical stability. Still, the algorithm is particularly necessary to improve the overall computational efficiency; otherwise, the z dependence of the coupled space harmonics will be harsh enough to require a large number of Legendre basis functions, the retaining of which can considerably enlarge the size of the involved matrices. This is especially pronounced in the analysis of metallic gratings used in TM polarization, gratings with a large contrast in their permittivity profile, or thick gratings.

3. COMPARISON AMONG RCWA, DM, AND LPEM

The proposed LPEM, the DM, and the RCWA algorithm all solve almost the same set of differential equations and can be fairly compared against one another. This comparison is here made by the analysis of two surface relief gratings with a sinusoidal profile of groove depth whose specifications, in accordance with Fig. 1, read as $2d=\lambda=\Lambda_G=1\ \mu$m, $n_1=1$, and $\alpha=15°$. In the first case, the refractive index of region 3 is $n_3=1.5$ and a dielectric sinusoidal grating, which is hereafter referred to as case A, is considered. In the second case, however, the refractive index of region 3 is $n_3=1-5j$ and a metallic sinusoidal grating, which is hereafter referred to as case B, is dealt with.

The required run times of the DM, the RCWA, and the LPEM to achieve an accuracy of 1% in the largest diffraction efficiency of both major polarizations in the above-mentioned cases are given in Table 1. All the numerical results are obtained by using MATLAB on a PC (Intel Core 2 Duo at 2 GHz and 1 Gbyte of RAM).

This table clearly shows that the proposed LPEM can outperform both the DM and the RCWA. However, to further demonstrate the superiority of the LPEM, the achieved relative error in the largest diffraction efficiency of case A used in TE polarization is plotted in Fig. 2 versus the elapsed run time of the DM (circles), the RCWA (triangles), and the LPEM (diamonds). In this figure, the total number of kept space harmonics is fixed at $2N+1=21$ for all of the above-mentioned algorithms. The reference value for the calculation of the relative error is obtained by using the C-method with $2N+1=201$ space harmonics, and then the accuracy of the DM, the RCWA, and the LPEM is improved by increasing the number of numerical steps used in the integration scheme, the number of slices in the staircase approximation, and the total number of Legendre polynomial basis functions (LM), respectively. It should be noticed that in this calculation M, i.e., the number of Legendre basis functions within each slice, is fixed at 6. This figure clearly demonstrates that the LPEM outpaces the DM and the RCWA in achieving the lowest error level that could be possibly obtained by

Table 1. Required Run Times of the DM, RCWA, and LPEM to Achieve an Accuracy of 1% in the Largest Diffraction Efficiency of Both Major Polarizations

	Required Run Time (s)		
Approach	DM [11]	RCWA [5]	LPEM
Case A			
TE polarization	0.042	0.008	0.004 with $L=1$
TM polarization	0.063	0.031	0.015 with $L=1$
Case B			
TE polarization	0.117	0.100	0.039 with $L=2$
TM polarization	3.08	Very large	0.62 with $L=17$

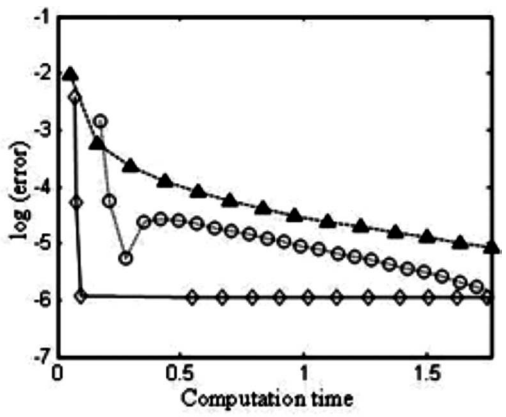

Fig. 2. Computational efficiency of the DM (circles), the RCWA (triangles), and the LPEM (diamonds).

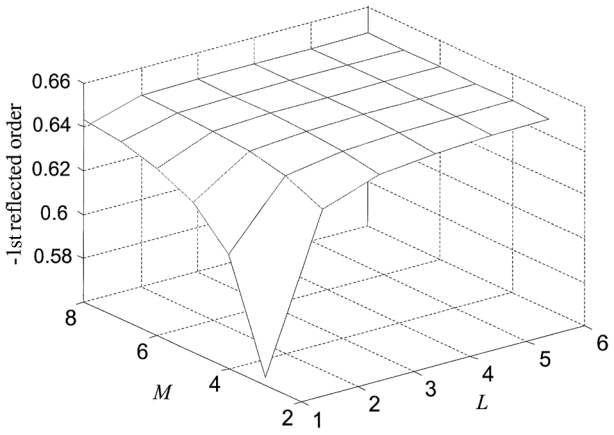

Fig. 3. TE polarized −1st reflected order of the metallic surface relief grating in case B versus L and M in applying the LPEM with $N=15$.

keeping $2N+1=21$ space harmonics. This is not unexpected, as spectral analysis using polynomial expansion is known to outperform many other techniques in solving ordinary differential equations [20,21].

Moreover, the diffraction efficiencies of the aforementioned surface relief gratings are examined to probe the accuracy and the convergence rate of the proposed method. The transmitted diffraction efficiencies of the −1st, the zeroth, and the +1st orders, together with the total diffraction efficiency of the dielectric surface relief grating in case A, are all summarized in Table 2, where the proposed LPEM with $N=5$, $M=6$, and different values of L is employed for both TE and TM polarizations. This table clearly shows that increasing L can improve the energy balance of the calculated diffraction efficiencies This is particularly true in TE polarization, for which $L=5$ is high enough to ensure that the energy balance criterion is satisfied within a precision of about 10^{-8}. In applying the DM, however, more than 1000 integration steps are needed to achieve the same precision. Such a high level of accuracy in holding the energy balance criterion is not observed for TM polarization, where $L=50$ cannot render a precision of better than 10^{-4}. It should be nonetheless noticed that better results are not obtained by using the conventional DM, and this somewhat low level of precision is in real fact due to the FFF technique, which is applied to improve the overall convergence speed. Fortunately, the truncation order N in applying the proposed LPEM method can be increased to improve the energy balance and to push the total diffraction efficiency further toward 1. For example applying the LPEM with $N=20$, $M=6$, and $L=50$ for the analysis of the same problem in TM polarization renders a precision of about 10^{-6}, i.e., a total diffraction efficiency of 0.99999665.

Additionally, the lossy metallic grating in case B is more closely examined, and plots of the convergence char-

Table 2. Transmitted Diffraction Efficiencies of the −1st, 0th, and +1st Orders, Together with the Total Diffracted Energy of the Dielectric Surface Relief Grating in Case A, Are All Calculated Using the LPEM with $N=5$ and $M=6$ and for Different Values of L

	Transmitted Efficiency			
L	−1st Order	0th Order	+1st Order	Total Diffracted Energy
TE				
1	0.1280789	0.6966239	0.1588289	1.000063246582
2	0.1281937	0.6963942	0.1588820	1.000001134920
3	0.1281940	0.6963924	0.1588828	1.000000192145
5	0.1281939	0.6963922	0.1588828	1.000000002966
10	0.1281939	0.6963922	0.1588828	0.999999999649
20	0.1281939	0.6963922	0.1588828	0.999999999985
TM				
1	0.8127049×10^{-1}	0.8439878	0.6706024×10^{-1}	1.000178730737
2	0.8194206×10^{-1}	0.8426590	0.6751512×10^{-1}	0.999942117523
3	0.8196372×10^{-1}	0.8426111	0.6753589×10^{-1}	0.999940711633
5	0.8195612×10^{-1}	0.8426233	0.6752787×10^{-1}	0.999936680417
10	0.8196147×10^{-1}	0.8426197	0.6752998×10^{-1}	0.999939591549
20	0.8196113×10^{-1}	0.8426203	0.6752963×10^{-1}	0.999939765866
50	0.8196109×10^{-1}	0.8426203	0.6752963×10^{-1}	0.999939766240

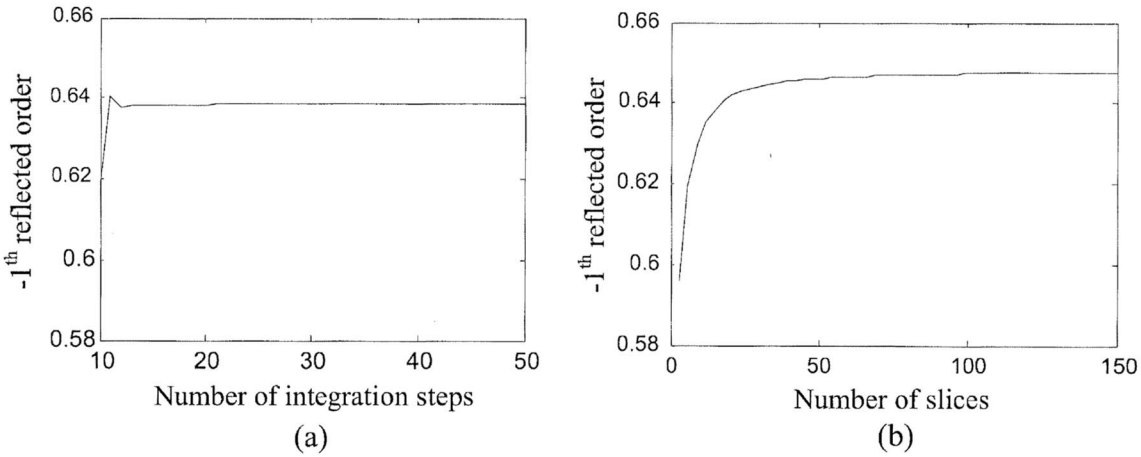

Fig. 4. TE-polarized −1st reflected order of the metallic surface relief grating in case B (a) versus the number of integration steps in applying the DM with $N=15$ (b) versus the number of slices in the staircase approximation based on the RCWA with $N=15$.

acteristic of the largest diffraction efficiency are provided, where the total number of kept space harmonics is truncated at $2N+1=31$. In TE polarization, the results obtained by using the proposed LPEM are presented in Fig. 3, where the −1st reflected order is plotted versus both M and L. For the sake of comparison, the DM and the staircase approximation based on the RCWA are employed to plot the convergence characteristics in Figs. 4(a) and 4(b), respectively. Along the same lines, the proposed LPEM, this time for the TM polarization, is applied and the convergence characteristic is presented in Fig. 5, where the zeroth reflected order is plotted versus M and L. Inasmuch as the staircase approximation is not valid for this case in the TM polarization [9], the convergence characteristic of the RCWA is not presented; yet, that of the DM is shown in Fig. 6, where the zeroth reflected order is plotted versus the number of integration steps.

4. COMPARISON BETWEEN C-METHOD AND LPEM

The LPEM, much like the DM and the RCWA, is a Fourier expansion method to solve the coupled set of differential equations governing the Fourier coefficients of the field components in a Cartesian system. The C-method, on the other hand, is a coordinate-transformation-based differential method that introduces a nonorthogonal curvilinear coordinate system that maps corrugated profiles to planar surfaces. It is indeed a fast and efficient strategy, which is applicable to arbitrary-shaped surface relief gratings with smooth and differentiable functions of groove depth. In this section, the computational efficiency of the C-method and that of the LPEM are compared against each other.

In the first working example, the aforementioned cases A and B are reconsidered, and the required run times to achieve an accuracy of 1% in the largest diffraction efficiency are given in Table 3. In these cases, the surface relief profile is sufficiently smooth and can be very effectively analyzed by using the C-method. The efficiency of the LPEM is, however, comparable to that of the C-method except for the metallic sinusoidal grating used in TM polarization. This latter case cannot be analyzed unless the whole structure is decomposed into $L=17$ subgratings.

In the second case in point, symmetric trapezoidal surface relief gratings with base angle $\theta=63.43°$ are analyzed. Similarly, both dielectric and metallic types are considered. In case C, a dielectric substrate with $n_3=1.5$

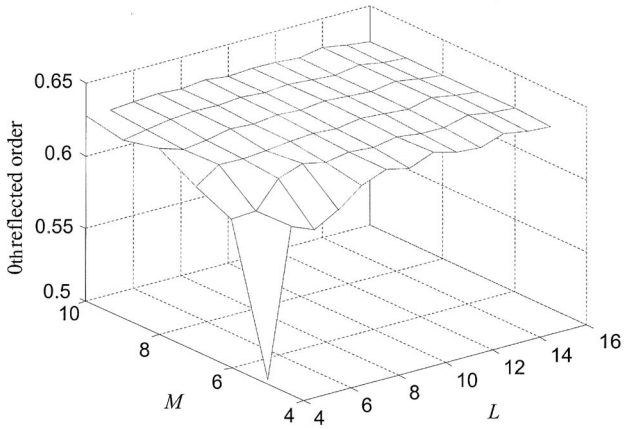

Fig. 5. TM-polarized zeroth reflected order of the metallic surface relief grating in case B versus L and M in applying the LPEM with $N=15$.

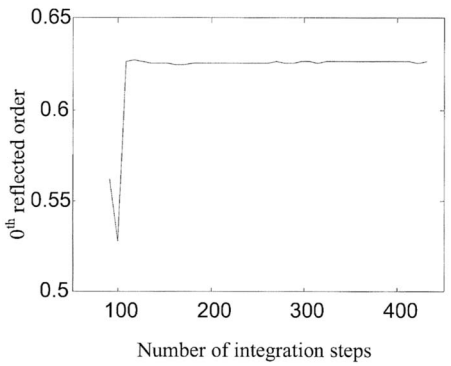

Fig. 6. TM-polarized zeroth reflected order of the metallic surface relief grating in case B versus the number of integration steps in applying the DM with $N=15$.

Table 3. Required Run Times of the C-Method and LPEM to Achieve an Accuracy of 1% in the Largest Diffraction Efficiency of Both Major Polarization in Cases A and B

	Required Time (s)		
Approach	C-Method	Single-Layer LPEM [18]	Multilayer LPEM
Case A			
TE polarization	0.008 with $N=4$	0.004 with $N=1$, $M=5$	0.004 with $N=1$, $M=5$, $L=1$
TM polarization	0.008 with $N=4$	0.007 with $N=1$, $M=4$	0.015 with $N=1$, $M=4$, $L=1$
Case B			
TE polarization	0.008 with $N=4$	0.043 with $N=6$, $M=8$	0.039 with $N=6$, $M=5$, $L=2$
TM polarization	0.005 with $N=3$	Very large	0.62 with $N=10$, $M=3$, $L=17$

Table 4. Required Run Rimes of the C-Method and LPEM to Achieve and Accuracy of 1% in the Largest Diffraction Efficiency of Both Major Polarizations in Cases C and D

	Required Time (s)		
Approach	C-Method	Single-Layer LPEM [18]	Multilayer LPEM
Case C			
TE polarization	0.051 with $N=10$	0.004 with $N=2$, $M=4$	0.004 with $N=2$, $M=4$, $L=1$
TM polarization	0.045 with $N=10$	0.004 with $N=1$, $M=3$	0.006 with $N=1$, $M=3$, $L=1$
Case D			
TE polarization	0.011 with $N=5$	0.007 with $N=3$, $M=5$	0.007 with $N=3$, $M=5$ $L=1$
TM polarization	6.61 with $N=62$	58 with $N=17$, $M=35$	1.77 with $N=17$, $M=3$, $L=16$

is worked out, and in case D, a metallic substrate with $n_3=1-5j$ is substituted for the dielectric. All other specifications are similar to those of the previous study cases A and B. The required run times to achieve an accuracy of 1% in the largest diffraction efficiency in the analysis of these two latter cases are then tabulated in Table 4. This time, the multilayer LPEM wins the upper hand, as the trapezoidal surface profile in these cases happens to be nondifferentiable and cannot be effectively analyzed with the C-method unless the adaptive spatial resolution technique is employed [15].

Table 5. Incurred Reciprocity Error in Applying the LPEM for the Analysis of Different Surface Relief Gratings in Cases A–D

Case	Reciprocity Error, e	Parameters
Case A		
TE polarization	1.998×10^{-9}	$N=5$, $M=6$, $L=2$
TM polarization	2.095×10^{-10}	$N=5$, $M=6$, $L=2$
Case B		
TE polarization	1.114×10^{-9}	$N=15$, $M=6$, $L=20$
TM polarization	1.128×10^{-10}	$N=15$, $M=6$, $L=20$
Case C		
TE polarization	8.334×10^{-6}	$N=5$, $M=6$, $L=2$
TM polarization	2.214×10^{-6}	$N=5$, $M=6$, $L=2$
Case D		
TE polarization	6.996×10^{-10}	$N=15$, $M=6$, $L=20$
TM polarization	6.403×10^{-6}	$N=15$, $M=6$, $L=20$

Consequently, the proposed LPEM cannot outperform the C-method if surface relief gratings with high-contrast permittivity profiles and differentiable functions of groove depth are to be analyzed. On the other hand, discontinuous profiles, volume gratings, and surface relief gratings with inhomogeneously filled grooves cannot be directly analyzed with the C-method. The latter case, however, can be analyzed by using an extension of the conventional C-method [22]. All these cases, however, have been successfully and directly analyzed by applying the proposed LPEM [18].

The calculated results of all these structures are then verified against the reciprocity theorem [1]. Here the following reciprocity error parameter, e, is defined to measure the symmetry of the calculated diffraction efficiencies:

$$e=\frac{\|DE^0(\theta)-DE^0(-\theta)\|}{\|DE^0(\theta)\|}, \tag{44}$$

where $DE^0\theta$ stands for the reflected zeroth-order diffraction efficiency as a function of the incident angle θ and the $\|\cdot\|$ sign stands for the L^2 norm. Insofar as the zeroth-order diffraction efficiency should be symmetrical with respect to the incident angle, the above-mentioned error parameter is ideally expected to be zero. This is tested in Table 5, where the reciprocity error parameter, e, is numerically calculated for all the preceding cases A–D. The incurred error, though nonzero, is small enough to exonerate the proposed LPEM.

At the end of this section, a sinusoidal metallic grating made of aluminum ($n_{Al}=1.3-7.6j$) is considered to present how the resonant scattering can be dealt with.

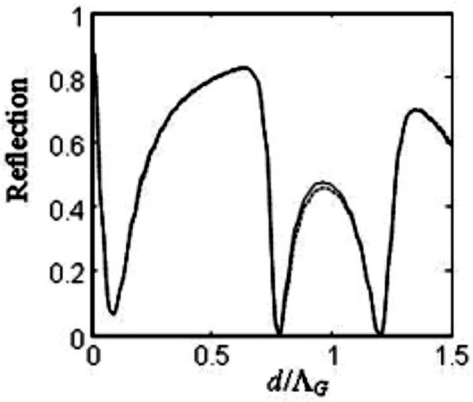

Fig. 7. Resonance anomaly in the TM reflectivity of a sinusoidal aluminum grating: LPEM with $N=20$, $M=3$, $L=150$ (solid curve), and the C-method (dashed curve).

The grating period is $\Lambda_G=0.5\ \mu$m, the incident wave illuminates the grating from air at $\theta=14.929°$, and the free-space wavelength is $\lambda=0.6328\ \mu$m [1]. The overall reflectivity of this structure as a function of the grating thickness is plotted in Fig. 7, where both the LPEM (solid curve) and the C-method (dashed curve) are applied. Despite the resonant anomalies, an excellent agreement is observed between the proposed LPEM and the C-method [1].

5. CONCLUSION

The LPEM is here generalized for the efficient analysis of arbitrary-shaped surface relief gratings. The modulated region is decomposed into a few sufficiently thin inhomgeneous slices of equal spatial period, wherein electromagnetic field dependence is smooth enough to be approximated by keeping a small number of Legendre polynomial basis functions. A rigorous approach is then followed, and the R-matrix propagation algorithm is applied to the Legendre polynomial expansion of the space harmonics. In this fashion, the size of the involved matrices is reduced and the overall performance of the LPEM is considerably enhanced. Different working examples are considered to evaluate the computational efficiency of the proposed approach against those of the DM, the RCWA, and the C-method.

APPENDIX A: CONSTRUCTION OF Q, χ, AND Ψ MATRICES

The $\mathbf{Q}$ matrix represents the algebraic projection of Maxwell's equations onto the linear space spanned by the Legendre basis functions. It is a $2(2N+1)(M-1)\times 2(2N+1)M$ matrix whose nonzero elements read as

$$\mathbf{Q}^{TE}(n+(i+N)(M-1)+1,m+(i+N)M+(2N+1)M+1) = -jk_0\langle P_n,P_m\rangle, \tag{A1}$$

$$\mathbf{Q}^{TE}(n+(i+N)(M-1)+(2N+1)(M-1)+1,m+(p+N)M+1) = -jk_0\left\langle P_n,\left([[\epsilon]]-\left(\frac{\mathbf{K_x}}{k_0}\right)^2\right)_{ip}P_m\right\rangle, \tag{A2}$$

$$\mathbf{Q}^{TE}(n+(i+N)(M-1)+1,m+(i+N)M+1) = \frac{2}{d_l}\langle P_n,P'_m\rangle, \tag{A3}$$

$$\mathbf{Q}^{TE}(n+(i+N)(M-1)+(2N+1)(M-1)+1,m+(i+N)M+(2N+1)M+1) = \frac{2}{d_l}\langle P_n,P'_m\rangle, \tag{A4}$$

for TE polarization, and

$$\mathbf{Q}^{TM}(n+(i+N)(M-1)+1,m+(p+N)M+1) = \langle P_n,\mathbf{M}_{ip}^{TM11}P_m\rangle, \tag{A5}$$

$$\mathbf{Q}^{TM}(n+(i+N)(M-1)+1,m+(p+N)M+(2N+1)M+1) = \langle P_n,\mathbf{M}_{ip}^{TM12}P_m\rangle, \tag{A6}$$

$$\mathbf{Q}^{TM}(n+(i+N)(M-1)+(2N+1)(M-1)+1,m+(p+N)M+1) = \langle P_n,\mathbf{M}_{ip}^{TM21}P_m\rangle, \tag{A7}$$

$$\mathbf{Q}^{TM}(n+(i+N)(M-1)+(2N+1)(M-1)+1,m+(p+N)M+(2N+1)M+1) = \langle P_n,\mathbf{M}_{ip}^{TM22}P_m\rangle, \tag{A8}$$

$$\mathbf{Q}^{TM}(n+(i+N)(M-1)+1,m+(i+N)M+1) = \frac{2}{d_l}\langle P_n,P'_m\rangle, \tag{A9}$$

$$\mathbf{Q}^{TM}(n+(i+N)(M-1)+(2N+1)(M-1)+1,m+(i+N)M+(2N+1)M+1) = \frac{2}{d_l}\langle P_n,P'_m\rangle, \tag{A10}$$

for TM polarization.

The $\boldsymbol{\chi}$ and $\boldsymbol{\psi}$ matrices have the following form for both major polarizations:

$$\boldsymbol{\chi} = \begin{bmatrix} \mathbf{0} & \chi_{12} \\ \mathbf{0} & \chi_{22} \end{bmatrix}, \tag{A11}$$

$$\boldsymbol{\psi} = \begin{bmatrix} \chi_{12} & \mathbf{0} \\ \chi_{22} & \mathbf{0} \end{bmatrix}, \tag{A12}$$

where

$$\chi_{12}(i+N+1,m+(i+N)M+1) = 1, \tag{A13}$$

$$\chi_{22}(i+N+1,m+(i+N)M+1) = (-1)^m. \tag{A14}$$

Please notice that indices n, m, i, and p run from 0 to $M-2$, 0 to $M-1$, $-N$ to N, and $-N$ to N, respectively.

ACKNOWLEDGMENT

The authors acknowledge the partial support of the Iran Telecommunication Research Center.

REFERENCES

1. E. G. Loewen and E. Popov, *Diffraction Gratings and Applications* (Marcel Dekker, 1997).
2. M. G. Moharam and T. K. Gaylord, "Rigorous coupled-wave analysis of planar-grating diffraction," J. Opt. Soc. Am. **71**, 811–818 (1981).
3. M. G. Moharam and T. K. Gaylord, "Three-dimensional vector coupled-wave analysis of planar-grating diffraction," J. Opt. Soc. Am. **73**, 1105–1112 (1983).
4. L. Li, "Formulation and comparison of two recursive matrix algorithms for modeling layered diffraction gratings," J. Opt. Soc. Am. A **13**, 1024–1035 (1996).
5. M. G. Moharam, D. A. Pommet, E. B. Grann, and T. K. Gaylord, "Stable implementation of the rigorous coupled-wave analysis for surface-relief gratings: Enhanced transmittance matrix approach," J. Opt. Soc. Am. A **12**, 1077–1086 (1995).
6. Ph. Lalanne and G. M. Morris, "Highly improved convergence of the coupled wave method for TM polarization," J. Opt. Soc. Am. A **13**, 779–784 (1996).
7. G. Garnet and B. Guizal, "Efficient implementation of the coupled wave method for metallic lamellar gratings in TM polarization," J. Opt. Soc. Am. A **13**, 1019–1023 (1996).
8. L. Li, "Use of Fourier series in the analysis of discontinuous periodic structures," J. Opt. Soc. Am. A **13**, 1870–1876 (1996).
9. E. Popov, M. Nevière, B. Gralak, and G. Tayeb, "Staircase approximation validity for arbitrary-shaped gratings," J. Opt. Soc. Am. A **19**, 33–42 (2002).
10. M. Nevière and E. Popov, *Light Propagation in Periodic Media: Differential Theory and Design* (Marcel Dekker, 2003).
11. E. Popov and M. Nevière, "Grating theory: New equations in Fourier space leading to fast converging results for TM polarization," J. Opt. Soc. Am. A **17**, 1773–1784 (2000).
12. J. Chandezon, D. Maystre, and G. Raoult, "A new theoretical method for diffraction gratings and its numerical application," J. Opt. (Paris) **11**, 235–241 (1980).
13. L. Li, J. Chandezon, G. Granet, and J. P. Plumey, "Rigorous and efficient grating-analysis method made easy for optical engineers," Appl. Opt. **38**, 304–403 (1999).
14. L. Li and J. Chandezon, "Improvement of the coordinate transformation method for surface-relief gratings with sharp edges," J. Opt. Soc. Am. A **13**, 2247–2255 (1996).
15. G. Granet, J. Chandezon, J. P. Plumey, and K. Raniriharinosy, "Reformulation of the coordinate transformation method through the concept of adaptive spatial resolution. Application to trapezoidal gratings," J. Opt. Soc. Am. A **18**, 2102–2108 (2001).
16. S. D. Gedney and R. Mittra, "Analysis of the electromagnetic scattering by thick gratings using a combined FEM/MM solution," IEEE Trans. Antennas Propag. **39**, 1605–1614 (1991).
17. M. Chamanzar, K. Mehrany, and B. Rashidian, "Planar diffraction analysis of homogeneous and longitudinally inhomogeneous gratings based on Legendre expansion of electromagnetic fields," IEEE Trans. Antennas Propag. **54**, 3686–3694 (2006).
18. A. Khavasi, K. Mehrany, and B. Rashidian, "Three-dimensional diffraction analysis of gratings based on legendre expansion of electromagnetic fields," J. Opt. Soc. Am. B **24**, 2676–2685 (2007).
19. L. Li and C. W. Haggans, "Convergence of the coupled wave method for metallic lamellar diffraction gratings," J. Opt. Soc. Am. A **10**, 1184–1189 (1993).
20. P. Sarrafi, N. Zareian, and K. Mehrany, "Analytical extraction of leaky modes in circular slab waveguides with arbitrary refractive index profile," Appl. Opt. **46**, 8656–8667 (2007).
21. J. P. Boyd, *Chebyshev and Fourier Spectral Methods*, 2nd ed. (Dover, 2001).
22. G. Granet, J. Chandezon, and O. Coudert, "Extension of the C method to nonhomogeneous media: Application to nonhomogeneous layers with parallel modulated faces and to inclined lamellar gratings," J. Opt. Soc. Am. A **14**, 1576–1582 (1997).